

**Orientation dependence of high-order harmonic generation in nanowire**Jiapeng Li,<sup>1</sup> Qingbin Zhang,<sup>1,\*</sup> Liang Li,<sup>1</sup> Xiaosong Zhu,<sup>1</sup> Tengfei Huang,<sup>1</sup> Pengfei Lan,<sup>1,†</sup> and Peixiang Lu<sup>1,2</sup><sup>1</sup>*School of Physics and Wuhan National Laboratory for Optoelectronics, Huazhong University of Science and Technology, Wuhan 430074, China*<sup>2</sup>*Hubei Key Laboratory of Optical Information and Pattern Recognition, Wuhan Institute of Technology, Wuhan 430205, China*

(Received 4 January 2019; published 27 March 2019)

We investigate the orientation dependence of high-order harmonic generation (HHG) in nanowires by solving the time-dependent Schrödinger equation. It is found that the harmonic spectrum exhibits a two-plateau structure and the two plateaus have different orientation dependences. The harmonic yield of the first plateau reaches a maximum when the laser field is parallel to the nanowire and gets a strong suppression when the laser field is perpendicular to the nanowire. The harmonic yield of the second plateau increases first and reduces eventually with the change of the nanowire orientation. These phenomena can be explained by the time-dependent population imaging and the analysis of the transition probability between different energy bands. Our analysis shows a strong band-sensitive orientation dependence in low-dimensional material.

DOI: [10.1103/PhysRevA.99.033421](https://doi.org/10.1103/PhysRevA.99.033421)**I. INTRODUCTION**

With the rapid development of laser technology, many interesting strong-field phenomena have been revealed over the past decades. One of the most fascinating phenomena is high-order harmonic generation (HHG) [1,2]. HHG from gas has been studied widely over the past several decades [3–8] due to it promises many important applications like generating the coherent XUV radiation [9–12] and exploring the ultrafast dynamics of atoms and molecules [13–16].

Recently, the experimental observation of HHG from bulk solids has attracted extensive attention [17–20]. Besides the same advantages as the gas HHG, the solid HHG also provides a new approach to reconstruct the energy band of solids [21] and to study the structures of solid materials [22,23]. Recent works have shown that the harmonic spectra from solids exhibit a two-plateau structure [24–26]. The two-plateau structure is attributed to the multiband structure of the solid [27]. The first plateau originates from the interband current between the valence band and the first conducting band, while the second plateau is attributed to the interband current between the valence band and the higher-lying second conducting band [25].

Compared with bulk solid, low-dimensional materials exhibit unique optical and electrical properties [28,29]. Recently, Liu *et al.* [30] show that high-order harmonics can be detected from a monolayer MoS<sub>2</sub> crystal. Compared with the HHG in bulk materials, the harmonic efficiency is increased from thin monolayer MoS<sub>2</sub>. High-order harmonic generation emitted from graphene has also been explored [31]. It is demonstrated that HHG is enhanced by elliptically polarized light excitation, and the resultant harmonic radiation has a

particular polarization. Furthermore, McDonald *et al.* [32] theoretically explore the harmonic generation of nanowires. It is shown that the quantum confinement provides an approach to increase the harmonic efficiency. However, the exploration is based on the laser polarization parallel to nanowires. As is well known, with the anisotropic structure, HHG from gas-phase molecules exhibits abundant interesting features and implies many intriguing applications due to the additional degree of freedom of the molecular orientation [33–35]. In this work, we focus on the orientation dependence of HHG in nanowires. It is shown that the harmonic spectrum has a two-plateau structure. The harmonic yield of the first plateau decreases gradually with the change of the nanowire orientation, and the harmonic yield of the second plateau increases first and reduces eventually. The results are explained based on the time-dependent population imaging (TDPI) [36] and the analysis of the transition probability [37] between different energy bands.

**II. THEORETICAL MODEL**

To investigate the orientation dependence of HHG in nanowire, we numerically solve the two-dimensional (2D) time-dependent Schrödinger equation (TDSE). In the length gauge with the dipole approximation, the time-dependence Hamiltonian is (atomic units are used unless stated otherwise)

$$\hat{H}(t) = \hat{H}_0 + \mathbf{r} \cdot \mathbf{F}(t), \quad (1)$$

where  $\hat{H}_0$  is the field-free Hamiltonian and  $\mathbf{F}(t)$  is the electric field of the driving laser.  $\hat{H}_0$  is written as  $\hat{H}_0 = \hat{p}^2/2 + V(\mathbf{r})$ , where  $\hat{p}$  is the momentum operator and  $V(\mathbf{r})$  is the lattice potential of the nanowire.

The 2D potential  $V(x, y) = -V_0(1 - \cos 2\pi x/a_x)(1 - \cos 2\pi y/a_y)$  is used to describe the unit lattice potential of the nanowire with  $V_0 = 0.5$  a.u. and  $a_x = a_y = 6$  a.u. These parameters are chosen such that the band gap of the periodic

\*zhangqingbin@hust.edu.cn

†pengfeilan@mail.hust.edu.cn

system is close to that of MgO [25]. Nanowire is a quasi-one-dimensional material with a periodic dimension and another finite dimension. For the periodic dimension  $x$ , we set 121 lattices, which is enough to ensure the periodicity of the nanowire. For the finite dimension  $y$ , we set 11 lattices. We also perform the simulation by changing the lattice number from 5 to 35 in the finite dimension and the same conclusions can be obtained. All calculations are performed in the coordination space with  $x$  region  $[-375, 375]$  a.u. and  $y$  region  $[-51, 51]$  a.u.  $\theta$  is defined as the orientation angle between the laser polarization and the nanowire.  $\theta = 0^\circ$  denotes the laser polarization is parallel to the nanowire.  $\theta = 90^\circ$  denotes the laser polarization is perpendicular to the nanowire.

The energy band structure of the nanowire can be acquired by solving the eigenvalue equation of  $\hat{H}_0$  [36,38],

$$\hat{H}_0\varphi_n(x, y) = E_n\varphi_n(x, y), \quad (2)$$

where  $n$  is the eigenvalue number and  $\varphi_n(x, y)$  is the corresponding eigenfunction. The eigenstate populated at the top of the valence band is chosen as the initial state [36,38,39].

The evolution of the time-dependent wave function  $\psi(t)$  can be obtained by numerically solving the TDSE with the second-order split-operator method [40]. An absorbing boundary is used to eliminate the physical reflection at the edge of the grid. The wavelength of the driving laser is 1600 nm and the intensity is  $3.72 \text{ TW/cm}^2$ . A sine-squared laser envelope is adopted. The total duration of the laser pulse is 11 optical cycles. We also perform the simulation by changing the intensity from 3 to  $7 \text{ TW/cm}^2$  and the wavelength from 1600 to 2400 nm. The conclusions will not change.

The movement of electron in the laser field produces a current. The laser-induced current  $j(t)$  can be obtained from the time-dependent wave function:

$$j(t) = -\langle \psi(t) | \hat{p} | \psi(t) \rangle. \quad (3)$$

The harmonic spectra can be obtained by calculating the Fourier transform of the current:

$$H(\omega) \propto \left| \int j(t) e^{i\omega t} dt \right|^2. \quad (4)$$

To reduce the noise of the signal, we multiply  $j(t)$  with a Hanning window [38] before the Fourier transformation.

To obtain the TDPI picture of the HHG, we calculate the instantaneous population  $|C_n(t)|^2$  of the electron on each eigenstate

$$|C_n(t)|^2 = |\langle \varphi_n | \psi_n(t) \rangle|^2. \quad (5)$$

The transition dipole moment  $d_{mn}$  of a single charged particle from state  $m$  to state  $n$  can be written as

$$d_{mn} = -\langle \psi_n | r | \psi_m \rangle, \quad (6)$$

where  $r$  is the position of the particle.

### III. RESULTS AND DISCUSSION

Figure 1(a) shows the harmonic spectra at the orientations  $\theta = 0^\circ$ ,  $30^\circ$ , and  $90^\circ$ . The harmonic spectra exhibit a two-plateau structure. The first plateau has a cutoff at the 15th order. The second plateau has a cutoff at the 25th

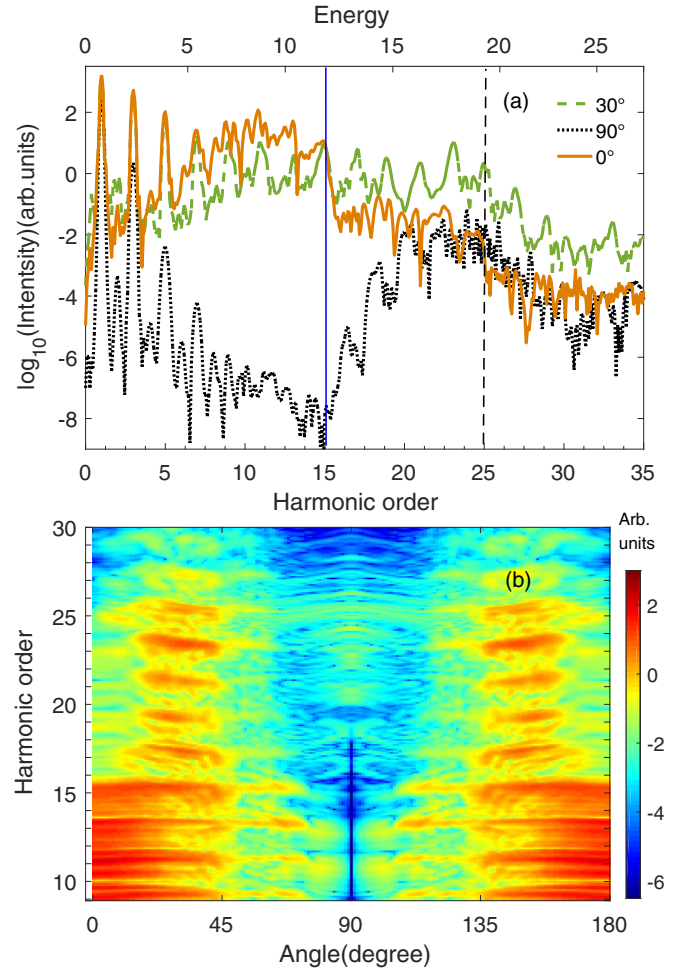


FIG. 1. (a) Harmonic spectra with  $0^\circ$  (brown line),  $30^\circ$  (green dashed line), and  $90^\circ$  (black dotted line), generated by a 1600-nm,  $3.72 \text{ TW/cm}^2$  laser pulse. The vertical blue solid (black dashed) line indicates the cutoff energy of the first (second) plateau. (b) Orientation dependence of the harmonic spectrum (shown in logarithmic scale).

order. In the first plateau, the intensity of the high-order harmonics with  $\theta = 0^\circ$  is higher than those with  $\theta = 30^\circ$  or  $90^\circ$ . In the second plateau, the intensity of the high-order harmonics with the  $\theta = 30^\circ$  orientation is highest. Moreover, the harmonic intensity of the first plateau is lower than that of the second plateau at the orientation  $\theta = 90^\circ$ . Figure 1(a) indicates that the HHG from the nanowire exhibits obvious orientation dependences and the orientation dependences are different for the two plateaus. To have a deeper insight into the orientation dependence, we calculate HHG spectra in other directions. The results are shown in Fig. 1(b). One can see that the orientation dependences of the two plateaus are symmetric about  $90^\circ$ . The harmonic intensity of the first plateau reaches a maximum at  $0^\circ$  and gets a strong suppression at  $90^\circ$ . In contrast, the harmonic intensity of the second plateau is peaked around  $30^\circ$ , which is very different from the first plateau.

To understand the mechanism of the HHG process in nanowire, we show the TDPI picture with  $\theta = 0^\circ$  in Fig. 2. The valence band is denoted as VB. The first and second conduction bands are denoted as CB1 and CB2, respectively.

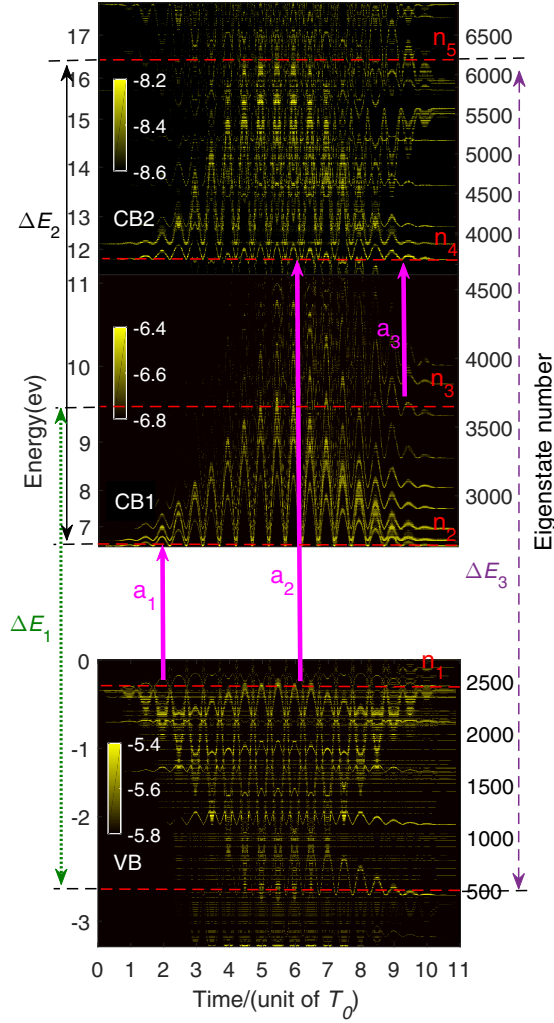


FIG. 2. The TDPI picture with  $0^\circ$ . In the TDPI picture, the horizontal red dashed lines indicate the highest and deepest eigenstate of the oscillating electrons in respective bands, which are denoted as the eigenstate number  $n_1$ ,  $n_2$ ,  $n_3$ , and  $n_4$ , respectively.  $\Delta E_1$ ,  $\Delta E_2$ , and  $\Delta E_3$  represent the maximum energy differences read from the TDPI picture.

The y coordinate on the right corresponds to the eigenstate number and the y coordinate on the left corresponds to the energy of the eigenstate. Initially, the electrons populate on VB. With the evolution of the laser field, the electrons populated on VB either oscillate or transit to CB1 and CB2. Likewise, the electrons on CB1 either oscillate or transit to CB2. The energy difference between the highest peak and deepest valley of population oscillations on CB1 and VB is  $\Delta E_1$  ( $\approx 12$  eV) and that on CB2 and CB1 is  $\Delta E_2$  ( $\approx 10$  eV). As shown in Fig. 1(a), the cutoff energy of the first plateau is about 12 eV. The transitions from CB1 to VB and the transitions from CB2 to CB1 can contribute to the first plateau. The energy difference between the highest peak and deepest valley of population oscillations on CB2 and VB is  $\Delta E_3$  ( $\approx 19$  eV), which is close to the cutoff energy of the second plateau. Therefore the transitions from CB2 to VB can contribute to the second plateau. In addition, the population of the oscillating electrons on CB2 is about two orders of magnitude lower than

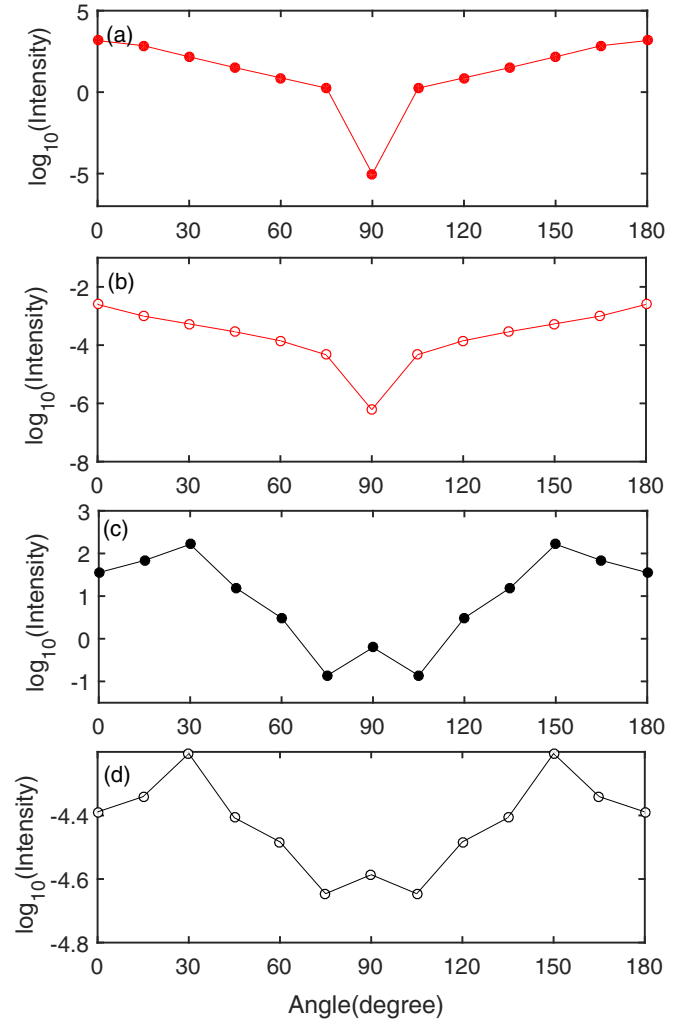


FIG. 3. (a) The orientation dependence of the harmonic yield of the first plateau. (b) The orientation dependence of average population on CB1 ( $P_1$ ). (c) The orientation dependence of the harmonic yield of the second plateau. (d) The orientation dependence of average population on CB2 ( $P_2$ ).

that on CB1, which makes the weak harmonic intensity of the second plateau interpreted.

To explain the orientation dependence of harmonic yield, we next explore the orientation dependence of the average population from the TDPI picture.  $P_1$  and  $P_2$  represent the average population for the oscillating electron in CB1 and CB2:

$$P_1 = \frac{1}{T(n_3 - n_2)} \sum_{n=n_2}^{n_3} \int_0^T dt |C_n(t)|^2, \quad (7)$$

$$P_2 = \frac{1}{T(n_5 - n_4)} \sum_{n=n_4}^{n_5} \int_0^T dt |C_n(t)|^2,$$

where  $n_2$ ,  $n_3$ ,  $n_4$ , and  $n_5$  are the maximum or minimum eigenstate numbers for the oscillating electrons as shown in Fig. 2.  $T$  is the total duration of the laser pulse.

Figures 3(a) and 3(b) exhibit the variation of the harmonic yield of the first plateau and the average population on CB1,

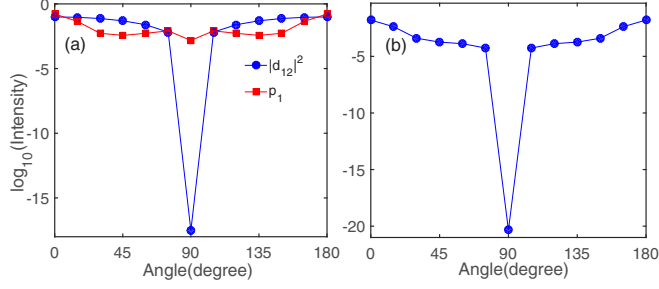


FIG. 4. (a) The orientation dependence of the population for eigenstate  $|n_1\rangle$  and the modular square of the transition dipole moment between  $|n_1\rangle$  and  $|n_2\rangle$ . (b) The orientation dependence of the transition probability ( $A_1$ ) from VB to CB1.

respectively. The orientation dependences of the harmonic yield of the second plateau and the average population on CB2 are presented in Figs. 3(c) and 3(d). These figures indicate that the harmonic yield and the population have a strong relevance. The more the electron populated, the higher the harmonic yield will be.

The orientation dependence of the average population can be further explained by the analysis of the transition probability. Since the band gap is smallest when the electron occupies the highest position of population oscillations, the transition probabilities among different bands can be predominantly expressed by the transition probabilities among the eigenstates  $|n_1\rangle$ ,  $|n_2\rangle$ ,  $|n_3\rangle$ , and  $|n_4\rangle$ , respectively. The population on CB1 is mainly contributed by the electrons transition from VB to CB1. We use  $a_1$  to represent this process in Fig. 2. The transition probability is represented by  $A_1$ ,

$$A_1 = p_1 |d_{12}|^2, \quad p_1 = \frac{1}{T} \int_0^T dt |C_{n_1}(t)|^2, \quad (8)$$

where  $d_{12}$  is the transition dipole moment between the eigenstate  $|n_1\rangle$  and  $|n_2\rangle$ .  $p_1$  is the population of the eigenstate  $|n_1\rangle$ .

As shown in Fig. 4(a), the population of  $|n_1\rangle$  (squares) changes slowly from  $\theta = 0^\circ$  to  $90^\circ$ , while the transition dipole moment  $d_{12}$  (circles) reduces gradually from  $\theta = 0^\circ$  to  $75^\circ$  and sharply drops around  $90^\circ$ . Under the combined effect of the strong orientation-dependent transition dipole momentum and the weak orientation-dependent population, the transition probability of the electron reaches a maximum under a laser field parallel to the nanowire, and gets a strong suppression when the polarization becomes perpendicular, as shown in Fig. 4(b).

The population on CB2 is mainly contributed by two channels: electrons pumped from VB to CB2 and electrons pumped from CB1 to CB2. These two processes are labeled by  $a_2$  and  $a_3$  in Fig. 2, respectively. The probability of the electron transition from VB and CB1 to CB2 is represented by  $A_2$ ,

$$A_2 = a_2 + a_3 = p_1 |d_{14}|^2 + p_3 |d_{34}|^2, \quad p_3 = \frac{1}{T} \int_0^T dt |C_{n_3}(t)|^2, \quad (9)$$

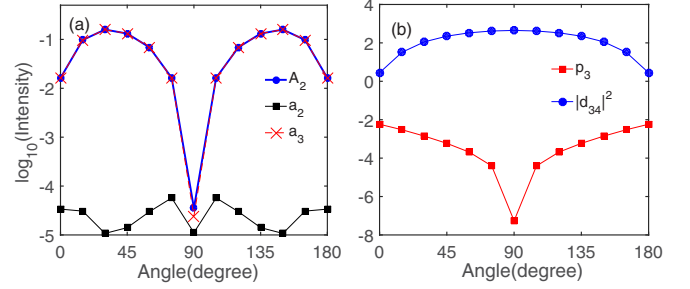


FIG. 5. (a) The orientation-dependent intensity of the transition probability ( $A_2$ ) from VB and CB1 to CB2 and the two channels  $a_2$  and  $a_3$ . (b) The orientation dependence of the population for  $|n_3\rangle$  and the modular square of the transition dipole moment between  $|n_3\rangle$  and  $|n_4\rangle$ .

where  $d_{14}$  is the transition dipole moment between the eigenstate  $|n_1\rangle$  and  $|n_4\rangle$ , and  $d_{34}$  denotes the transition dipole moment between the eigenstate  $|n_3\rangle$  and  $|n_4\rangle$ .  $p_3$  is the population of the state  $|n_3\rangle$ .

Figure 5(a) shows the orientation-dependent intensity for the transition probability  $A_2$  (circles),  $a_2$  (squares), and  $a_3$  (crosses). One can see that the electron transition from CB1 to CB2 is about three orders of magnitude larger than that from VB to CB2. Therefore the population on CB2 is dominated by the electrons transition from CB1 to CB2. The population of  $|n_3\rangle$  and the transition dipole moment between  $|n_3\rangle$  and  $|n_4\rangle$  are presented in Fig. 5(b). When  $\theta$  is less than  $30^\circ$ , the population of  $|n_3\rangle$  declines gently, meanwhile the dipole moment rises rapidly, which results in an upward trend of the transition probability of  $a_3$ . When  $\theta$  is larger than  $30^\circ$ , the population drops rapidly and the transition dipole moment increases slowly. Therefore, the transition probability of  $a_3$  peaks at  $\theta = 30^\circ$ .

#### IV. CONCLUSION

We explore the orientation dependence of HHG in nanowire based on a 2D single-electron model. It is shown that the orientation dependences of the first and second plateaus are different. Based on the analyses for the TDPI and the transition probability of the different energy bands, we show that the different orientation dependences of the two plateaus is due to the different orientation-dependent transition probabilities from VB to CB1 and CB2, respectively. Specifically, the electron prefers to be promoted to CB1 in parallel orientation, while the transition to CB2 is strongest around  $30^\circ$ . Our results show that the HHG yield in different plateaus is sensitive to the features of the respective conduction bands.

#### ACKNOWLEDGMENT

This work was supported by the National Natural Science Foundation of China under Grants No. 11774109, No. 11627809, and No. 11574101.

- [1] A. McPherson, G. Gibson, H. Jara, U. Johann, T. S. Luk, I. A. McIntyre, K. Boyer, and C. K. Rhodes, *J. Opt. Soc. Am. B* **4**, 595 (1987).
- [2] M. Ferray, A. L'Huillier, X. F. Li, L. A. Lompre, G. Mainfray, and C. Manus, *J. Phys. B* **21**, L31 (1988).
- [3] P. B. Corkum, *Phys. Rev. Lett.* **71**, 1994 (1993).
- [4] M. Lewenstein, P. Balcou, M. Y. Ivanov, A. L'Huillier, and P. B. Corkum, *Phys. Rev. A* **49**, 2117 (1994).
- [5] T. Brabec and F. Krausz, *Rev. Mod. Phys.* **72**, 545 (2000).
- [6] C. D. Lin, A. T. Le, Z. Chen, T. Morishita, and R. Lucchese, *J. Phys. B* **43**, 122001 (2010).
- [7] J.-P. Brichta, M. C. H. Wong, J. B. Bertrand, H.-C. Bandulet, D. M. Rayner, and V. R. Bhardwaj, *Phys. Rev. A* **79**, 033404 (2009).
- [8] X. Zhu *et al.*, *Opt. Express* **19**, 24198 (2011); X. Zhang *et al.*, *Phys. Rev. A* **99**, 013414 (2019); X. Zhu *et al.*, *Opt. Express* **20**, 16275 (2012); L. Li *et al.*, *Phys. Rev. Lett.* **120**, 223203 (2018).
- [9] P. M. Paul, E. S. Toma, P. Breger, G. Mullot, F. Auge, P. Balcou, H. G. Muller, and P. Agostini, *Science* **292**, 1689 (2001).
- [10] M. Hentschel *et al.*, *Nature (London)* **414**, 509 (2001).
- [11] G. Sansone *et al.*, *Science* **314**, 443 (2006).
- [12] T. S. Sarantseva, M. V. Frolov, N. L. Manakov, A. A. Silaev, N. V. Vvedenskii, and A. F. Starace, *Phys. Rev. A* **98**, 063433 (2018); K. Liu, S. Luo, M. Li, Y. Li, Y. Feng, B. Du, Y. Zhou, P. Lu, and I. Barth, *Phys. Rev. Lett.* **122**, 053202 (2019); C. Y. Zhai *et al.*, *Opt. Commun.* **437**, 104 (2019).
- [13] A. Schiffrin *et al.*, *Nature (London)* **493**, 70 (2013).
- [14] J. Itatani *et al.*, *Nature (London)* **432**, 867 (2004).
- [15] X.-B. Bian and A. D. Bandrauk, *Phys. Rev. Lett.* **113**, 193901 (2014).
- [16] L. He, P. Lan, A. T. Le, B. Wang, B. Wang, X. Zhu, P. Lu, and C. D. Lin, *Phys. Rev. Lett.* **121**, 163201 (2018); J. Tan, Y. Zhou, M. He, Y. Chen, Q. Ke, J. Liang, X. Zhu, M. Li, and P. Lu, *ibid.* **121**, 253203 (2018); R. Wang *et al.*, *Opt. Express* **27**, 6471 (2019).
- [17] S. Ghimire, A. D. DiChiara, E. Sistrunk, P. Agostini, L. F. DiMauro, and D. A. Reis, *Nat. Phys.* **7**, 138 (2010).
- [18] B. Zaks, R. B. Liu, and M. S. Sherwin, *Nature (London)* **483**, 580 (2012).
- [19] O. Schubert *et al.*, *Nat. Photonics* **8**, 119 (2014).
- [20] C. Yu, X. Zhang, S. Jiang, X. Cao, G. Yuan, T. Wu, L. Bai, and R. Lu, *Phys. Rev. A* **94**, 013846 (2016); S. Jiang, J. Chen, H. Wei, C. Yu, R. Lu, and C. D. Lin, *Phys. Rev. Lett.* **120**, 253201 (2018).
- [21] G. Vampa, T. J. Hammond, N. Thire, B. E. Schmidt, F. Legare, C. R. McDonald, T. Brabec, D. D. Klug, and P. B. Corkum, *Phys. Rev. Lett.* **115**, 193603 (2015).
- [22] M. Schultze *et al.*, *Science* **346**, 1348 (2014).
- [23] G. Vampa *et al.*, *Nature (London)* **522**, 462 (2015).
- [24] G. Ndabashimiye *et al.*, *Nature (London)* **534**, 520 (2016).
- [25] M. Wu, Y. You, S. Ghimire, D. A. Reis, D. A. Browne, K. J. Schafer, and M. B. Gaarde, *Phys. Rev. A* **96**, 063412 (2017).
- [26] T. Y. Du and X. B. Bian, *Opt. Express* **25**, 151 (2017).
- [27] P. G. Hawkins, M. Yu. Ivanov, and V. S. Yakovlev, *Phys. Rev. A* **91**, 013405 (2015); P. G. Hawkins and M. Yu. Ivanov, *ibid.* **87**, 063842 (2013).
- [28] R. R. Nair *et al.*, *Science* **320**, 1308 (2008); X. Li *et al.*, *ibid.* **324**, 1312 (2009); Y. Zhang *et al.*, *Nature (London)* **438**, 201 (2005).
- [29] J. Chen *et al.*, *Nano Lett.* **18**, 1344 (2018); W. W. Liu *et al.*, *Adv. Funct. Mater.* **28**, 1707550 (2018).
- [30] H. Liu, Y. Li, Y. S. You, S. Ghimire, T. F. Heinz, and D. A. Reis, *Nat. Phys.* **13**, 262 (2016).
- [31] N. Yoshikawa, T. Tamaya, and K. Tanaka, *Science* **356**, 736 (2017).
- [32] C. R. McDonald, K. S. Amin, S. Aalmalki, and T. Brabec, *Phys. Rev. Lett.* **119**, 183902 (2017).
- [33] P. M. Kraus, A. Rupenyan, and H. J. Wörner, *Phys. Rev. Lett.* **109**, 233903 (2012).
- [34] E. Frumker, C. T. Hebeisen, N. Kajumba, J. B. Bertrand, H. J. Wörner, M. Spanner, D. M. Villeneuve, A. Naumov, and P. B. Corkum, *Phys. Rev. Lett.* **109**, 113901 (2012).
- [35] Y. P. Li, S. J. Yu, W. Y. Li, and Y. J. Chen, *Phys. Rev. A* **95**, 063412 (2017).
- [36] X. Liu, X. Zhu, P. Lan, X. Zhang, D. Wang, Q. Zhang, and P. Lu, *Phys. Rev. A* **95**, 063419 (2017).
- [37] C. Yu, S. Jiang, T. Wu, G. Yuan, Z. Wang, C. Jin, and R. Lu, *Phys. Rev. B* **98**, 085439 (2018).
- [38] T. Huang, X. Zhu, L. Li, X. Liu, P. Lan, and P. Lu, *Phys. Rev. A* **96**, 043425 (2017).
- [39] T.-Y. Du, Z. Guan, X.-X. Zhou, and X.-B. Bian, *Phys. Rev. A* **94**, 023419 (2016).
- [40] M. D. Feit, J. A. Fleck, and A. Steiger, *J. Comput. Phys.* **47**, 412 (1982).